Title

Sulfur Dioxide Accelerates the Heterogeneous Oxidation Rate of Organic Aerosol by Hydroxyl Radicals

Journal

Environmental Science and Technology, 50(7)

ISSN

0013-936X

Authors

Richards-Henderson, NK
Goldstein, AH
Wilson, KR

Publication Date

2016-04-05

DOI

10.1021/acs.est.5b05369

Peer reviewed

Sulfur Dioxide Accelerates the Heterogeneous Oxidation Rate of Organic Aerosol by Hydroxyl Radicals

Authors: Nicole K. Richards-Henderson[1], Allen H. Goldstein[2] and Kevin R. Wilson[1*]

Affiliations:
[1]Chemical Sciences Division, Lawrence Berkeley National Laboratory, Berkeley, California 94720, USA

[2]Department of Environmental Science, Policy and Management, University of California Berkeley, Berkeley, California 94720, USA

*Correspondence to: krwilson@lbl.gov.

Abstract: There remains considerable uncertainty in how anthropogenic gas phase emissions alter the oxidative aging of organic aerosols in the troposphere. Here we observe a 10-20 fold acceleration in the effective heterogeneous OH oxidation rate of organic aerosol in the presence of SO_2. This acceleration originates from the radical chain reactions propagated by alkoxy radicals, which are formed efficiently inside the particle by the reaction of peroxy radicals with SO_2. As the OH approaches atmospheric concentrations, the radical chain length increases, transforming the aerosol at rates predicted to be up to 10 times the OH-aerosol collision frequency. Model predictions, constrained by experiments over orders of magnitude changes in [OH] and [SO_2], suggest that in polluted regions the heterogeneous processing of organic aerosols by OH ([SO_2] $\geq$ 40 ppb) occur on similar timescales as analogous gas-phase oxidation reactions. These results provide evidence for a previously unidentified mechanism by which organic aerosol oxidation is enhanced by anthropogenic gas phase emissions.

Introduction

Despite their small number density, organic aerosols (OA) are important constituents[1, 2] of the troposphere contributing to large scale impacts on climate,[3] air pollution and human health.[4] Accurate predictions of these impacts require a detailed understanding of all relevant multiphase chemical reaction mechanisms and timescales. Modeling the transformation chemistry of OA is challenging due in part to the large number of chemical species in an aerosol and the complex and potentially unidentified feedbacks between gas and particle phase chemistry, which include heterogeneous and photochemical reactions, condensed phase reactions and the condensation of low-volatility gas phase reaction products. Currently, many models under-predict the daily evolution of OA suggesting either unknown oxidation mechanisms or unknown gas-phase precursors.[5]

Secondary organic aerosol (SOA) is observed to form rapidly within hours after sunrise in contrast to the timescale of days for known heterogeneous oxidation reactions, whose rate is limited by the OH-particle collision frequency. Recently we reported evidence that free radical chain reactions lead to rapid acceleration of the effective heterogeneous oxidation rate of hydroxyl radicals (OH) in the presence of NO.[6] Here we investigate whether SO_2 can play an analogous role as NO in accelerating effective heterogeneous oxidation rates. Broadly this study is aimed at understanding how anthropogenic gas phase emissions alter organic aerosol oxidation pathways.

Shown in Fig. 1 is a simplified reaction mechanism for the reaction of saturated organic molecules (i.e. hydrocarbon, RH) with OH. The reaction begins at the aerosol surface by a reactive collision of OH (Fig. 1: R1), which abstracts a hydrogen atom from RH to form an alkyl radical (R) and water. This alkyl radical rapidly converts to a peroxy radical (RO_2) by reaction with O_2 (Fig. 1: R2). In the absence of both HO_2 and NO, RO_2 undergoes self-reactions (with other RO_2)

leading to the formation of stable products (ketone or alcohol, Fig. 1: R4) or alkoxy radicals (RO, Fig. 1 R3). The heterogeneous reaction rate is quantified as a reaction probability or reactive uptake coefficient (γ) and reflects the fraction of OH surface collisions that produce a reaction. Measuring the gas phase loss of OH to the aerosol surface yields an uptake coefficient (γ_{OH}) that is by definition ≤ 1 since the maximum rate is limited by the OH-surface collision frequency. Alternatively, the heterogeneous reaction can be measured via the decay of RH to obtain an effective uptake coefficient (γ_{eff}). Since γ_{eff} is sensitive to all reaction pathways that might consume RH (in addition to OH), effective uptake coefficients can in fact be larger than 1 in the presence of secondary radical chain chemistry.[7] For example, RO (Fig. 1: R5) can abstract H atoms from an organic molecule leading to an additional loss channel for RH.

Sulfur dioxide (SO_2) is a major anthropogenic pollutant with global emission rates of 65-90 Tg yr^{-1}[8]. In the U.S,[9] SO_2 is emitted by fossil fuel combustion at power plants (e.g. coal) and industrial facilities, by the oxidation of organic materials in soils, volcanic eruptions and biomass burning. While nitric oxide (NO) is readily oxidized in both the gas ($k = 8 \times 10^{-12}$ cm^3 $molecules^{-1}$ s^{-1}) and condensed ($k = 5 \times 10^{-12}$ cm^3 $molecules^{-1}$ s^{-1}) phases by RO_2,[10-12] the gas phase reaction $SO_2 + RO_2$ is observed to be much slower at room temperature, suggesting that this reaction plays only a minor role in atmospheric gas phase oxidation pathways. However some uncertainty[13] still remains as to the magnitude of the gas phase rate coefficient ($k \sim 10^{-14}$-10^{-17} cm^3 $molecules^{-1}$ s^{-1}) and mechanism (single vs. multistep) for the reaction of SO_2 with small peroxy radicals,[14, 15]

It was hypothesized by Ellison et al.,[16] that unlike the gas phase, RO_2 radicals may in fact react with SO_2 at an aerosol surface, since this reaction is more exothermic than the analogous RO_2 + NO reaction. To examine how SO_2 impacts heterogeneous OH oxidation rates, γ_{eff} was quantified using three organic aerosol proxies: squalane (Sq, $C_{30}H_{62}$, liquid), bis(2-ethylhexyl) sebacate

(BES, $C_{26}H_{50}O_4$, liquid) and triacontane (Tri, $C_{30}H_{62}$, solid). Kinetic measurements were conducted over many orders of magnitude in reaction time (37 seconds to hours) and reagent concentration: $\sim 2 \times 10^7 \leq [OH] \leq \sim 1 \times 10^{10}$ molec. cm^{-3}, 40 ppb $\leq [SO_2] \leq 2.3$ ppm.

Experimental

Organic aerosol is formed via homogeneous nucleation by passing dry N_2 over a heated reservoir (135 $^{\circ}$C) containing the organic. As the flow cools, particles nucleate in a log-normal size distribution with a mean surface-weighted diameter of ~160 ± 30 nm. The aerosol is then introduced into an atmospheric pressure flow-reactor (FTR) or a continuous flow stirred tank reactor (CFSTR), both of which are described in detail elsewhere.[17]

In both reactors, the aerosol is allowed to react with OH in 10% O_2 in both the presence and absence of SO_2 (Praxair, 45.8 ppm diluted in N_2) at a relative humidity of 30%. In the FTR, O_3 (the OH precursor) is directly introduced into the reactor and then photolyzed using 254 nm lamps (no 185 nm present in the FTR) to produce $O(^1D)$, which reacts with water vapor to form OH. In the CFSTR, OH radicals are formed by the 254 nm photolysis of O_3, which unlike the FTR, is generated *in situ.* This is done using a 230 mm long Hg pen ray lamp (UVP), whose length is covered by a type 219 quartz sleeve, which eliminates 185 nm radiation. 1-2 mm of the lamp length is left uncovered allowing a small fraction of 185 nm light to photolyze O_2 to make O_3 inside the reactor. Once produced, O_3 is photolyzed by the main 254 nm output of the lamp.

For select CFSTR experiments, black lights (~350 nm) were used to generate OH radicals from H_2O_2 instead of O_3. These experiments were used to check for possible photochemistry at 185 and/or 254 nm as well as unwanted side reactions with O_3 (the OH precursor). As detailed

below, we observed no evidence that photochemistry at either 185 or 254 nm or side reactions involving O_3 are responsible for the results reported here.

The particle size distributions (before and after reaction) were measured using a scanning mobility particle sizer (TSI, Inc.). The chemical composition of the aerosol was measured using a home-built tunable vacuum ultraviolet photoionization aerosol mass spectrometer (VUV-AMS), described previously.[7] The photoionization energy used in the majority of experiments is 10.2 eV produced by the Chemical Dynamics Beamline (9.0.2) at the Advanced Light Source located in Berkeley CA.

A portion of the flow exiting the reactor is filtered and sampled by a gas chromatograph with a flame ionization detector (SRI Instruments). The gas chromatograph was used to measure one of three possible gas-phase tracers (Praxair, 4.99 ppm hexane in N_2, 8 ppm hexanal in N_2, 5 ppm 2-methyl-2-butene in N_2) for determining OH exposure using a mixed phase relative rate method.[18] After dilution, the final tracer concentration in the reactors is between 300-500 ppb.

Kinetic Analysis

Heterogeneous kinetics are measured by monitoring the reactive decay of the parent ion in the VUV photoionization aerosol mass spectrum of Sq, BES, or Tri as a function of OH exposure in the flow-tube reactor. In the CFSTR the decay of the parent ion is measured as a function of reaction time, as described previously.[17] In the flow tube reactor an exponential fit to the parent decay, as shown for BES in Fig. 2, is used to determine an effective heterogeneous rate constant (k_{eff}).[17] This rate constant is then used to compute an effective uptake coefficient (γ_{eff}):

$$\gamma_{eff} = \frac{2 \cdot k_{eff} \cdot D_{surf} \cdot \rho_0 \cdot N_a}{\bar{c} \cdot 3 \cdot M} \quad (1)$$

where D_{surf} is the measured mean surface-weighted particle diameter, ρ_0 is density, N_a is Avogadro's number, $\bar{c}$ is the mean speed of gas-phase OH and M is the molecular weight. The analysis of the CFSTR data to obtain k_{eff} follows the procedure described in detail by Che et al.[17]

Fig. 2 shows an example of the normalized decay of BES aerosol versus OH exposure. In the presence of 2.3 ppm of SO_2 the decay of BES is observed to be much more rapid than the decay measured without SO_2. In the presence of 2.3 ppm of SO_2, γ_{eff} is computed to be 1.2 ± 0.18 compared with 0.53 ± 0.12 without SO_2. $\gamma_{eff} > 1$ shows that the reaction is 20% more rapid than the OH-aerosol collision frequency, providing clear evidence for particle-phase secondary chain chemistry first hypothesized by Ellison et al.[16]

A kinetic model of the data was formulated in Kinetiscope© an open access software package,[19] which uses stochastic algorithms for kinetic simulations. The reactions used in the model are illustrated in Fig. 1 and shown in Table 1. Additional model details can be found in section S1 of the supplemental information (SI).

Results and Discussion

Fig. 3a-c shows γ_{eff} as a function of $[SO_2]$ for Sq, BES and Tri at $[OH]_{avg} = 10^8$ and 10^{10} molec. cm^{-3}. γ_{eff} is observed to increase with increasing $[SO_2]$, which is more pronounced at the lower OH concentration. For example, both Sq and BES exhibit γ_{eff} in excess of 1 at $[SO_2]$ = ~200 ppb and $[OH] = 10^8$ molec. cm^{-3}. This is in contrast with $[OH]_{avg} = 10^{10}$ molec. cm^{-3} where γ_{eff} is observed to be less that one for all $[SO_2]$ except 2.3 ppm ($\gamma_{eff} > 1$). At all [OH], the solid Tri particles exhibit a similar trend as the liquid particles, although the overall increase in γ_{eff} is much more gradual presumably due to mass transfer limitations in solid particles.[20, 21]

It is clear from Fig. 3 that in addition to SO_2, the absolute OH concentration plays a significant role in determining the magnitude of γ_{eff}. Shown in Fig. 4a-c, are measurements of γ_{eff} vs. [OH] at $[SO_2]$ = 84 ± 22 ppb. As [OH] decreases from 10^{10} to 10^7 molec. cm^{-3} there is a substantial increase in γ_{eff}. The functional form of γ_{eff} vs. [OH] in the presence of SO_2 is nearly identical to that observed in our previous NO study, suggesting similar chain propagation mechanisms.[7] At [OH] = 2×10^7 molec. cm^{-3} in the presence of SO_2, γ_{eff} for Sq and BES is 1.8 and 3.3, respectively. These values are ~5 times larger than at [OH] = 10^{10} molec. cm^{-3}. For comparison, Fig. 4 shows measurements conducted in the absence of SO_2 (labeled OH only), which do not exhibit a strong dependence on [OH].

Also shown in Fig. 4a and b are CFSTR measurements conducted using black lights (λ ~ 350 nm) and H_2O_2 as the OH precursor. The values for $\gamma_{eff,}$ determined under these condition, are identical, within experimental error, to those conducted using O_3 as the OH precursor and 255/185 nm as the photolysis source. These results show that photochemistry at 254 and/or 185 nm and side reactions with O_3 (e.g. $RO_2 + O_3 \rightarrow RO + 2O_2$) are not responsible for the accelerated oxidation rates observed in Fig. 3 and 4. Specifically, this eliminates the possibility that the chain propagation reactions originate from the 185 nm photolysis of SO_2 to form highly reactive SO radicals and O atoms.

During the reaction with SO_2 present, a new particle distribution was observed. These new particles were identified by long path FTIR to be H_2SO_4; produced via the following reactions:[22]

$$SO_2 + OH + M \rightarrow SO_2{\cdot}OH + M \quad (2)$$

$$SO_2{\cdot}OH + O_2 \rightarrow SO_3 + HO_2 \quad (3)$$

$$SO_3 + H_2O + M \rightarrow H_2SO_4 + M \quad (4)$$

Previous investigations have suggested that alcohols can react with H_2SO_4 leading to alkyl sulfate formation.[23] Thus the enhancement in γ_{eff} observed in Figs. 3 and 4 could in principle arise from acid-catalyzed aerosol-phase reactions, since it is currently not known whether acidic aerosols could catalyze radical chain propagation chemistry.

To examine this possibility, H_2SO_4 particles were coated with either Sq or BES and allowed to react with OH in the absence of SO_2. Particles were generated by atomizing a 5 mM solution of H_2SO_4 with a mean surface diameter of 95 nm. A coating thickness (D_{OA}) of either Sq or BES was then applied by passing the aerosol through an oven containing the organic. The organic coating thickness was determined from the difference in the mean surface diameter of the particle distribution before (D_{H2SO4}) and after coating ($D_{OA + H2SO4}$). Based on the insolubility of Sq and BES in water we assume that the organic coated H_2SO_4 particles adopt a core-shell morphology.

Fig. 5 shows that decay rate of Sq or BES (k_{eff}) decreases with thicker organic coatings. k_{eff} is observed to decrease as 1/r since the oxidation of thinner coatings proceeds more rapidly due to the larger concentration of reactant available at the surface relative to the bulk. To determine if aerosol acidity plays a role in the heterogeneous oxidation, γ_{eff} is computed from k_{eff} using Eq. (1) as shown in Fig. 5. γ_{eff} is observed to be, within error, identical to that of pure Sq or BES and independent of coating thickness, providing evidence that H_2SO_4 formed in the reaction is not contributing to the accelerated chemistry observed in Figs. 3 and 4.

Another possible source for the enhanced oxidation rate observed in Figs. 3 and 4 is reaction of the triplet excited states of SO_2, which have been known to oxidize gas-phase alkanes

in the atmosphere. The formation of triplet excited states begins with the absorption of UV light by SO_2:

$$SO_2 + h\nu \rightarrow {}^1SO_2^* \xrightarrow{ISC} {}^3SO_2^* \quad (5)$$

$${}^3SO_2^* + O_2 \rightarrow {}^1O_2^* + SO_2 \quad (6)$$

$${}^3SO_2^* + RH \rightarrow R^{\cdot} + HSO_2 \quad (7)$$

where ${}^1SO_2^*$ is the short-lived singlet excited state of SO_2 and ISC represents intersystem crossing. As illustrated by Eq. 7, ${}^3SO_2^*$ can abstract a hydrogen from RH producing an alkyl radical (R), thus initiating a free radical chain.

To evaluate the possibility that ${}^3SO_2^*$ could be reacting with our model compounds, Sq particles in our FTR were illuminated with 254 nm light and the parent ion signal was monitored as a function of [SO_2]. These measurements were conducted without the OH precursor added to the reactor (Fig. S3). No statistically significant difference in the Sq ion signal was observed with increasing concentrations of SO_2. Eq. 6 shows that ${}^3SO_2^*$ and ${}^1O_2^*$ are intricately tied since ground state oxygen is typically the largest sink for triplet excited states. Based on these measurements we observe no experimental evidence that reactions of either ${}^3SO_2^*$ or ${}^1O_2^*$ contributes to the enahnced heterogeneous oxidation rates observed in Figs. 3 and 4.

Since no evidence was observed that H_2SO_4 or the triplet excited states of SO_2 (${}^3SO_2^*$) play any role in the accelerated reaction rates observed in Figs. 3 and 4, we developed a kinetic model, which assumes the observed enhancement of γ_{eff} originates from free radical chain propagation chemistry. Two models are developed to explore differing assumptions regarding the mechanism of the $RO_2 + SO_2$ reaction, which previously in the gas phase has been considered to proceed either

in a single step or via the formation of adducts in multiple steps.[15] First, we developed a kinetic model (R1-R6), which assumes that the SO_2 + RO_2 reaction occurs in a single step to produce a RO radical or potentially organic sulfates. This reaction scheme is exactly analogous to the mechanism recently reported by us for heterogeneous reactions of OH with OA in the presence of NO.[6] The rate coefficients in the model are from previous literature and are shown in Table 1.[6, 15, 24, 25] The branching ratio for the RO_2 self-reaction (R4) and (R3) to form either a carbonyl-alcohol pair or two RO· are fixed at 90:10, respectively, and are based upon a previous study.[26] As shown recently in the gas phase by Crounse et al.,[27] hydroperoxides (ROOH) could be formed at low [OH] via a RO_2 auto-oxidation mechanism. Although, ROOH species were not detected in the aerosol mass spectrum, they could, if formed, be photolyzed in the reactor to form RO and OH, which could propagate a chain reaction. We tested this possibility in our model using rate constants reported by Crounse et al.[27] over a range of realistic photolysis rate constants for ROOH (7×10^{-5} s^{-1} to 10^{-2} s^{-1}). Including this pathway in the model produces results that were indistinguishable from those when this reaction is neglected. Thus under our experimental conditions the dominate sink for RO_2 radicals appear to be via reactions with either RO_2 or SO_2.

Monodisperse aerosol size measurements, in which the surface-to-volume ratio of the particles was varied (Fig. S4), show that the RO_2 + SO_2 reaction occurs within the interior of the aerosol and not at its surface. Therefore, in the model the [SO_2] in the aerosol phase is fixed by a unit-less Henry's law constant of 164 ± 11, consistent with previous measurements.[28, 29] The only adjustable parameter in the single step model is the RO_2 + SO_2 rate constant (R6), which leads to either RO or an organic sulfate. The formation of an organic sulfates is a chain termination product, which would not lead to an overall increase in heterogeneous oxidation rate. We observed no evidence of the formation of organic sulfates in our VUV photoionization aerosol mass spectra or

in additional measurements using a softer ionization technique (DART-MS) as well as long-path FTIR. Furthermore, we were not able to identify any peaks in the mass spectrum originating from dissociative photoionization of organic sulfates (e.g. elimination of H_2SO_4). Thus it appears that the $RO_2 + SO_2$ reaction produces exclusively RO radicals. This is also consistent with our recent results that found no evidence for particle phase alkyl nitrate formation from the $RO_2 + NO$ reaction.[6] Thus, in the model only the $RO_2 + SO_2$ rate constant was varied to replicate all of the results shown in Figs. 3 and 4. Shown as solid lines in Figs. 3 and 4, the model shows reasonable agreement with the experimental results using a $RO_2 + SO_2$ rate constant of $(2.1 \pm 0.4) \times 10^{-13}$ cm^3 molec.$^{-1}$ s^{-1}. For reference, this rate constant is 30 times slower than the value obtained for the model of the aerosol phase $RO_2 + NO$ reaction (i.e. 6.5×10^{-12} cm^3 molec.$^{-1}$ s^{-1}).[6] Tri particles were not modeled here, since to accurately describe heterogeneous reactions in solid particles requires explicit treatment of diffusion pathways in a spatially resolved reaction-diffusion model.

The particle-phase $RO_2 + SO_2$ rate constant used to replicate experiment is four orders of magnitude larger than the value obtained for the gas-phase (~10^{-17} cm^3 molec.$^{-1}$ s^{-1}).[14] This large increase in the particle-phase rate constant is unexpected since energy barriers of elementary reactions should be similar to those in the gas-phase. Therefore a multi-step adduct formation mechanism for $RO_2 + SO_2$, proposed by Kan et al.,[15] was evaluated in a second model (R1-R5, R7a-e). The multistep mechanism has a more complex dependence on $[O_2]$ and $[RO_2]$ than the single step $RO_2 + SO_2$ mechanism. In this model, R7a, the rate coefficient for the initial RO_2SO_2 adduct formation, is varied to replicate the experimental data in Figs. 3 and 4. The subsequent steps (R7b-e) are fixed at the values reported in Kan et al.[15] The model results (dashed lines in Figs. 3 and 4) show good agreement with experimental results using a value of 1.1×10^{-13} cm^3 molec.$^{-1}$ s^{-1} for R7a. Even though both the single step (R6) and multi-step models (R7a-e) can

replicate our experimental results, the particle-phase rate constant for R7a is only one order of magnitude larger than the gas-phase value (1.6×10^{-14} cm^3 $molec.^{-1}$ s^{-1}) reported by Kan et al.[15] for the reaction of methyl peroxy radicals with SO_2. This difference in rate coefficient for the initial adduct formation may not be that surprising given the large differences in molecular structure of the peroxy radicals (methyl vs. C_{30}) and environments (i.e. gas vs. solvent cage in the organic aerosol phase.) Thus, it seems likely that the more complex multi-step reaction mechanism is a more reasonable description of the chemistry occurring inside the aerosol studied here.

The experimental and model results indicate that γ_{eff} is controlled by the competition between the RO_2 + SO_2 (chain propagating to form RO) and chain terminating RO_2 + RO_2 reactions. This is seen in Fig. 4 in which there is a clear inverse relationship between γ_{eff} and the absolute [OH] at constant SO_2 (84 ± 22 ppb). At high [OH] (10^8 – 10^{10} molecules cm^{-3}) the particle phase RO_2 concentration is also relatively high so that the loss of RO_2 is mainly by reactions with other RO_2 to form stable chain terminating products. This is further illustrated in Fig. 3 in which a higher concentration of SO_2 is needed at [OH] = 10^{10} molecules cm^{-3} to obtain the same γ_{eff} as observed at [OH] = 10^8 molecules cm^{-3}. Lower OH concentrations (10^6 – 10^7 molecules cm^{-3}) leads to a reduction in RO_2 (whose consumption rate scales as $[RO_2]^2$) thereby favoring reaction with SO_2. The SO_2 + RO_2 reaction forms RO, which reacts with nearby molecules by H abstraction to reform R and eventually RO_2. These peroxy radicals can react again with SO_2 to generate another RO radical thereby increasing γ_{eff} by radical chain propagation. The coproduct of the RO_2 + SO_2 reaction is SO_3 (Fig. 1). Subsequent reactions of SO_3 are not explicitly included in the model, but we expect that the dominant sink for this species will be via reaction with H_2O to form H_2SO_4 in the particle (see Eq. (4)). As shown in Fig. 5, there is no evidence that the formation of this additional H_2SO_4 contributes to the accelerated reaction kinetics.

The model, constrained by experiment, can be extrapolated to global average atmospheric OH conditions (2×10^6 molecules cm^{-3}) as shown in Fig. 4. At low [OH] γ_{eff} of BES and Sq are predicted to be 10.6 and 3.4, respectively. These heterogeneous oxidation rates are 10-20 times faster than with OH alone. It should be noted that these results and model interpretation are consistent with accelerated heterogeneous reactions in the presence of NO recently reported by us.[6] In that case, the chain propagation step is the same; the reaction of RO_2 with NO to form alkoxy radicals. In the NO study, free radical chain reactions accelerated oxidation rates for Sq and BES by 10 to 50 times at [OH] = 2×10^6 molecules cm^{-3} and [NO] = ~80 ppb.[7] Though the increase in the rate of heterogeneous oxidation in the presence of SO_2 is more modest (due to the smaller rate coefficient for $RO_2 + SO_2$ step) compared to NO, together these results illustrate that anthropogenic gas phase emissions of SO_2 and NO can significantly accelerate the heterogeneous aging of organic aerosols in the atmosphere.

To evaluate the significance of the $SO_2 + RO_2$ reaction in the atmosphere, the model was run using SO_2 concentrations reported by the Environment Protection Agency.[30] Fig. 6 shows predicted γ_{eff} (Sq and BES) as a function of SO_2 (10-60 ppb) for daytime ground levels of OH ranging from (1 -8) $\times 10^6$ molecules cm^{-3}. As expected, γ_{eff} increases with higher SO_2 concentrations and is inversely proportional to OH concentration, in agreement with the measured trends presented in Figs. 3 and 4. However, even at much lower SO_2 concentrations (20 ppb) γ_{eff} remains larger than 1 for both Sq and BES.

By comparing the kinetic lifetimes of gas and particle phase alkanes, the relative importance of the $RO_2 + SO_2$ reaction can be estimated. The heterogeneous lifetime of an alkane (i.e. squalane)[17] in a 150-nm diameter particle with a γ_{eff} of 0.3 in a remote region (absence of

SO_2), is 4 days, assuming a global mean [OH] of 2×10^6 molec. cm^3. The kinetic lifetime of an analogous gas-phase alkane (e.g. dodecane, $C_{12}H_{26}$) is 11 hours (k = 1.32 x 10^{-11} cm^3 $molecules^{-1}$ s^{-1}). In the presence of SO_2 (10 to 60 ppb) the chain propagation mechanism accelerates heterogeneous oxidation reaction rates by 2 to 9 times the OH collision frequency (Fig. 6). Thus, we predict in polluted environments where SO_2 concentrations range from 10 to 60 ppb and [OH] = 2×10^6 molec. cm^3, the heterogeneous lifetime ranges from 9 to 43 hours; timescales that are comparable to the gas-phase lifetime of dodecane. These results also suggest that regional fluctuations in gas phase SO_2 concentrations will lead to relatively large changes in heterogeneous oxidation rates during the lifetime of the aerosol in the atmosphere. From Fig. 6, we expect that heterogeneous oxidation rates will be most sensitive to [SO_2] at low [OH] < 2 x 10^6 molec. cm^{-3}.

Atmospheric Implications

This work and our previous[6] study reveal how anthropogenic SO_2 and NO emissions can significantly accelerate heterogeneous OH oxidation through radical chain propagation reactions. This propagation chemistry leads to much shorter time scales for heterogeneous transformations of particle phase organics than previously expected and its importance should be evaluated in chemical transport models. Although these experiments are for simple single component OA proxies, the SO_2 + RO_2 mechanism could be general and important for oxidative aging of primary aerosol emissions (e.g. diesel emissions).[31] However, it remains unclear how this mechanism might transform more highly oxygenated secondary organic aerosol constituents, since chemically activated alkoxy radicals would be the products of the RO_2 + SO_2 reaction. Unimolecular decomposition of activated alkoxy radicals[26] can effectively compete with bimolecular H abstraction reactions, thus enhancing aerosol fragmentations reactions in the presence of SO_2 and NO. Future work is needed to evaluate the importance of C-C scission reactions in the presence

of SO_2 and NO as well as the potential importance of free radical cycling in more dilute aqueous solutions and semi-solids in order to better understand the role that molecular structure and particle phase has on chain cycling chemistry. Finally, these results suggests further work is needed to understand whether aerosol phase peroxy radicals are important sinks for NO or SO_2. In particular, it is unclear whether the oxidation of SO_2 by RO_2 inside OA could be an important mechanism for sulfate formation.

Supporting Information: The Supporting Information is available free of charge on the ACS Publications website. A detailed discussion of stochastic modeling and Figs. S1-S4 are provided.

Acknowledgments: This work and the Advanced Light Source were supported by the Director, Office of Energy Research, Office of Basic Energy Science of the U.S. Department of Energy under Contract No. DE-AC02-05CH11231. K.R.W was supported by the Department of Energy, Office of Science Early Career Research Program. We thank Dr. Frances Houle and Dr. Aaron Wiegel for technical support on the model and Mr. Bruce Rude for technical support on the instrument. We acknowledge Dr. Michael Ward for work on initial experiments.

References

1. Zhang, Q.; Jimenez, J. L.; Canagaratna, M. R.; Allan, J. D.; Coe, H.; Ulbrich, I.; Alfarra, M. R.; Takami, A.; Middlebrook, A. M.; Sun, Y. L., et al., Ubiquity and dominance of oxygenated species in organic aerosols in anthropogenically-influenced Northern Hemisphere midlatitudes. *Geophys. Res. Lett.* **2007,** *34*, (13), L13801.

2. Murphy, D. M.; Cziczo, D. J.; Froyd, K. D.; Hudson, P. K.; Matthew, B. M.; Middlebrook, A. M.; Peltier, R. E.; Sullivan, A.; Thomson, D. S.; Weber, R. J., Single-particle mass spectrometry of tropospheric aerosol particles. *J. Geophys. Res.-Atmos* **2006,** *111*, (D23), D23S32.

3. Stocker, T. F.; Qin, D.; Plattner, G.-K.; Tignor, M.; Allen, S. K.; Boschung, J.; Nauels, A.; Xia, Y.; Bex, V.; Midgley, P. M., IPCC, 2013: Climate change 2013: The physical science basis. Contribution of working group I to the fourth assessment report of the intergovernmental panel on climate change *Cambridge University Press, Cambridge, United Kingdom and New York, NY, USA.* **2013**.

4. Pope, C. A.; Ezzati, M.; Dockery, D. W., Fine-Particulate Air Pollution and Life Expectancy in the United States. *N. Engl. J. Med.* **2009,** *360*, (4), 376-386.

5. Jimenez, J. L.; Canagaratna, M. R.; Donahue, N. M.; Prevot, A. S. H.; Zhang, Q.; Kroll, J. H.; DeCarlo, P. F.; Allan, J. D.; Coe, H.; Ng, N. L., et al., Evolution of Organic Aerosols in the Atmosphere. *Science* **2009,** *326*, (5959), 1525-1529.

6. Richards-Henderson, N. K.; Goldstein, A. H.; Wilson, K. R., Large Enhancement in the Heterogeneous Oxidation Rate of Organic Aerosols by Hydroxyl Radicals in the Presence of Nitric Oxide. *J. Phys. Chem. Lett.* **2015,** *6*, (22), 4451-4455.

7. Liu, C.-L.; Smith, J. D.; Che, D. L.; Ahmed, M.; Leone, S. R.; Wilson, K. R., The direct observation of secondary radical chain chemistry in the heterogeneous reaction of chlorine atoms with submicron squalane droplets. *Phys. Chem. Chem. Phys.* **2011,** *13*, (19), 8993-9007.

8. Levin, Z.; Cotton, W. R., *Aerosol Pollution Impact on Precipitation: A Scientific Review*. Springer: 2009.

9. http://www3.epa.gov/airquality/sulfurdioxide/

10. Goldstein, S.; Lind, J.; Merenyi, G., Reaction of Organic Peroxyl Radicals with •NO2 and •NO in Aqueous Solution: Intermediacy of Organic Peroxynitrate and Peroxynitrite Species. *J. Phys. Chem. A* **2004,** *108*, (10), 1719-1725.

11. Abbatt, J.; Oldridge, N.; Symington, A.; Chukalovskiy, V.; McWhinney, R. D.; Sjostedt, S.; Cox, R. A., Release of Gas-Phase Halogens by Photolytic Generation of OH in Frozen Halide-Nitrate Solutions: An Active Halogen Formation Mechanism? *J. Phys. Chem. A.* **2010,** *23*, (114), 6527-6533.

12. Eberhard, J.; Howard, C. J., Rate Coefficients for the Reactions of Some C3 to C5 Hydrocarbon Peroxy Radicals with NO. *J. Phys. Chem. A* **1997,** *101*, (18), 3360-3366.

13. Lightfoot, P. D.; Cox, R. A.; Crowley, J. N.; Destriau, M.; Hayman, G. D.; Jenkin, M. E.; Moortgat, G. K.; Zabel, F., Organic peroxy radicals: Kinetics, spectroscopy and tropospheric chemistry. *Atmos. Environ.* **1992,** *26*, (10), 1805-1961.

14. Sander, S. P.; Watson, R. T., A kinetics study of the reaction of SO2 with CH3O2. *Chem. Phys. Lett.* **1981,** *77*, (3), 473-475.

15. Kan, C. S.; Calvert, J. G.; Shaw, J. H., Oxidation of sulfur dioxide by methylperoxy radicals. *J. Phys. Chem.* **1981,** *85*, (9), 1126-1132.

16. Ellison, G. B.; Tuck, A. F.; Vaida, V., Atmospheric processing of organic aerosols. *J. Geophys. Res.: Atmos* **1999,** *104*, (D9), 11633-11641.

17. Che, D. L.; Smith, J. D.; Leone, S. R.; Ahmed, M.; Wilson, K. R., Quantifying the reactive uptake of OH by organic aerosols in a continuous flow stirred tank reactor. *Phys. Chem. Chem. Phys.* **2009,** *11*, (36), 7885-7895.

18. Hearn, J. D.; Smith, G. D., A mixed-phase relative rates technique for measuring aerosol reaction kinetics. *Geophys. Res. Lett.* **2006,** *33*, (17), L17805.

19. Hinsberg, W. D.; Houle, F. A., Kinetiscope a stochastic kinetics simulator. *available under a no-cost license from www.hinsberg.net/kinetiscope* **2015**.

20. Renbaum, L. H.; Smith, G. D., The importance of phase in the radical-initiated oxidation of model organic aerosols: reactions of solid and liquid brassidic acid particles. *Phys. Chem. Chem. Phys.* **2009,** *11*, (14), 2441-2451.

21. Ruehl, C. R.; Nah, T.; Isaacman, G.; Worton, D. R.; Chan, A. W. H.; Kolesar, K. R.; Cappa, C. D.; Goldstein, A. H.; Wilson, K. R., The Influence of Molecular Structure and Aerosol Phase on the Heterogeneous Oxidation of Normal and Branched Alkanes by OH. *J. Phys. Chem. A* **2013,** *117*, (19), 3990-4000.

22. Atkinson, R.; Baulch, D. L.; Cox, R. A.; Crowley, J. N.; Hampson, R. F.; Hynes, R. G.; Jenkin, M. E.; Rossi, M. J.; Troe, J., Evaluated kinetic and photochemical data for atmospheric chemistry: Volume I - gas phase reactions of Ox, HOx, NOx and SOx species. *Atmos. Chem. Phys.* **2004,** *4*, (6), 1461-1738.

23. Levitt, N. P.; Zhao, J.; Zhang, R., Heterogeneous chemistry of butanol and decanol with sulfuric acid: Implications for secondary organic aerosol formation. *J. Phys. Chem. A* **2006,** *110*, (49), 13215-13220.

24. Denisov, E. T.; Afanas'ev, I. B., *Oxidation and Antioxidants in Organic Chemistry and Biology*. Taylor & Frances: 2005.

25. Houle, F. A.; Hinsberg, W. D.; Wilson, K. R., Oxidation of a model alkane aerosol by OH radical: the emergent nature of reactive uptake. *Phys. Chem. Chem. Phys.* **2015,** *17*, (6), 4412-4423.

26. Wiegel, A. A.; Wilson, K. R.; Hinsberg, W. D.; Houle, F. A., Stochastic methods for aerosol chemistry: a compact molecular description of functionalization and fragmentation in the heterogeneous oxidation of squalane aerosol by OH radicals. *Phys. Chem. Chem. Phys.* **2015,** *17*, (6), 4398-4411.

27. Crounse, J. D.; Nielsen, L. B.; Jørgensen, S.; Kjaergaard, H. G.; Wennberg, P. O., Autoxidation of Organic Compounds in the Atmosphere. *J. Phys. Chem. Lett.* **2013,** *4*, (20), 3513-3520.

28. Renon, H.; Lenoir, J. Y.; Renault, P., Gas chromatographic determination of Henry's constants of 12 gases in 19 solvents. *J. Chem. Eng. Data* **1971,** *16*, (3), 340-342.

29. Benoit, R. L.; Milanova, E., Vapour pressure and calorimetric data for the solution of sulfur dioxide in aprotic solvents. *Can. J. Chem.* **1979,** *57*, (11), 1319-1323.

30. http://www.epa.gov/airtrends/sulfur.html, In.

31. Worton, D. R.; Isaacman, G.; Gentner, D. R.; Dallmann, T. R.; Chan, A. W. H.; Ruehl, C.; Kirchstetter, T. W.; Wilson, K. R.; Harley, R. A.; Goldstein, A. H., Lubricating Oil Dominates

Primary Organic Aerosol Emissions from Motor Vehicles. *Environ. Sci. Technol.* **2014,** *48*, (7), 3698-3706.

32. Cocks, A. T.; Fernando, R. P.; Fletcher, I. S., The gas-phase reaction of the methylperoxy radical with sulphur dioxide. *Atmos. Environ.* **1986,** *20*, (12), 2359-2366.

Table 1: Reaction scheme and rate constants for kinetic simulations

no	Reaction[a]	k (cm^3 $molecules^{-1}$ s^{-1}) *unless otherwise noted*	Comment/Ref
R1	RH(n) + OH → R(n) + H_2O (n = 0-4)	–	[b]
R2	R(n) + O_2 → ROO(n) (n = 0-4)	6.23×10^{6}	24c
R3	2 ROO(n) → 2 RO(n)	1.00×10^{-16}	24
R4	ROO(n) + ROO(m) → RH(n+1) + RH(m+1) (n,m = 0-4)	4.00×10^{-15}	24
R5	RH + RO(n) →R(n+1) + R(n)	1.66×10^{-15}	24
R6	ROO(n) + SO_2 → RO(n) + SO_3	2.10×10^{-13}	d
R7a	ROO(n) + SO_2 → RO_2SO_2	1.1×10^{-13}	e
R7b	RO_2SO_2 → ROO(n) + SO_2	24 s^{-1}	15
R7c	RO_2SO_2 + O_2 ↔ $RO_2SO_2O_2$	see [f]	15,f
R7d	$RO_2SO_2O_2$ + ROO(n) → RO(n) + RO_2SO_2O	3.3×10^{-13}	15
R7e	RO_2SO_2O → ROO(n) + SO_3	10 s^{-1}	32

[a] A reaction diagram of this table is shown in Schematic 1. The letters *n* and *m* denote the number of oxygenated functional groups added to the squalane carbon backbone to form ketones or alcohols.
[b]Treated as pseudo first order where the average [OH] varies depending on experiment and k is from the experiment without added SO_2. Squalane for example has a k[OH] = 0.122 where k is 1.39 x 10^{-12} cm^3 $molecules^{-1}$ s^{-1} (γ = 0.27, d = 162 nm) and $[OH]_{avg} = 9.5 \times 10^{10}$ molecules cm^{-3}[17].
[c] Treated as pseudo first order where $[O_2]$ = 10%, $k = 2.5 \times 10^{-12}$ and the unit less Henry's law constant is 0.18.
[d] The $RO_2 + SO_2$ rate constant of 2.1×10^{-13} cm^3 $molecules^{-1}$ s^{-1} was determined by varying the pseudo first order rate constant ($k[SO_2]$) in order to best replicate the experimental data. The SO_2 concentration in the particle phase computed using the unit-less Henry's law constant, which is 164 ± 11[29], and the SO_2 concentration in the reactor.
[e] The $RO_2 + SO_2$ rate constant of 1.1×10^{-13} cm^3 $molecules^{-1}$ s^{-1} was determined by varying the pseudo first order rate constant ($k[SO_2]$) in order to best replicate the experimental data.
[f] From Kan et al.[15]: $k_{forward}$ $[O_2]/k_{backward}$ = 13 where $[O_2]$ is the current experimental value of 10%.

Fig. Legends:

Fig. 1. Generalized reaction scheme for the oxidation of saturated hydrocarbons by OH in the presence of SO_2.

Fig. 2. The reactive decay of BES as a function of OH exposure with (○) and without (●) SO_2.

Fig. 3. γ_{eff} as a function of [SO_2] for (a) Sq, (b) BES, and (c) Tri. at $[OH]_{avg} = 10^{10}$ molec. cm^{-3} (○) and 10^8 molec. cm^{-3} (●). Model predictions: (solid line) single step model (R6) and (dashed line) multi-step model (R7a-e) from Kan et al.[15] Arrow indicates the value for γ_{eff} without SO_2 (OH only).

Fig. 4. γ_{eff} as a function of [OH] with [SO_2] = 84 ± 22 ppb (●) and without (○) for: (a) Sq, (b) BES, and (c) Tri. The (blue, ▲) shows experiments conducted using black lights and H_2O_2 as the OH precursor. Model predictions: (solid line) single step model (R6) and (dashed line) multi-step model (R7a-e) from Kan et al.[15] Error bars represent ±1 SE (standard error) propagated from the standard errors of $k_{Hex,}$ k_{eff}, and particle diameter.

Fig. 5: γ_{eff} (solid symbols) and k_{eff} (open symbols) as a function of organic coating thickness on H_2SO_4 aerosol assuming a core-shell morphology for: (a) Sq and (b) BES. γ_{eff} and k_{eff} for pure Sq (a) and BES (b) aerosol are shown as (▲) and (□) respectively. Arrows delineate the respective axes. Lines show predicted 1/r dependence for k_{eff}. All measurements were conducted in the flow-tube reactor.

Fig. 6. Model predictions of γ_{eff} as a function of [OH] for several concentrations of [SO_2].

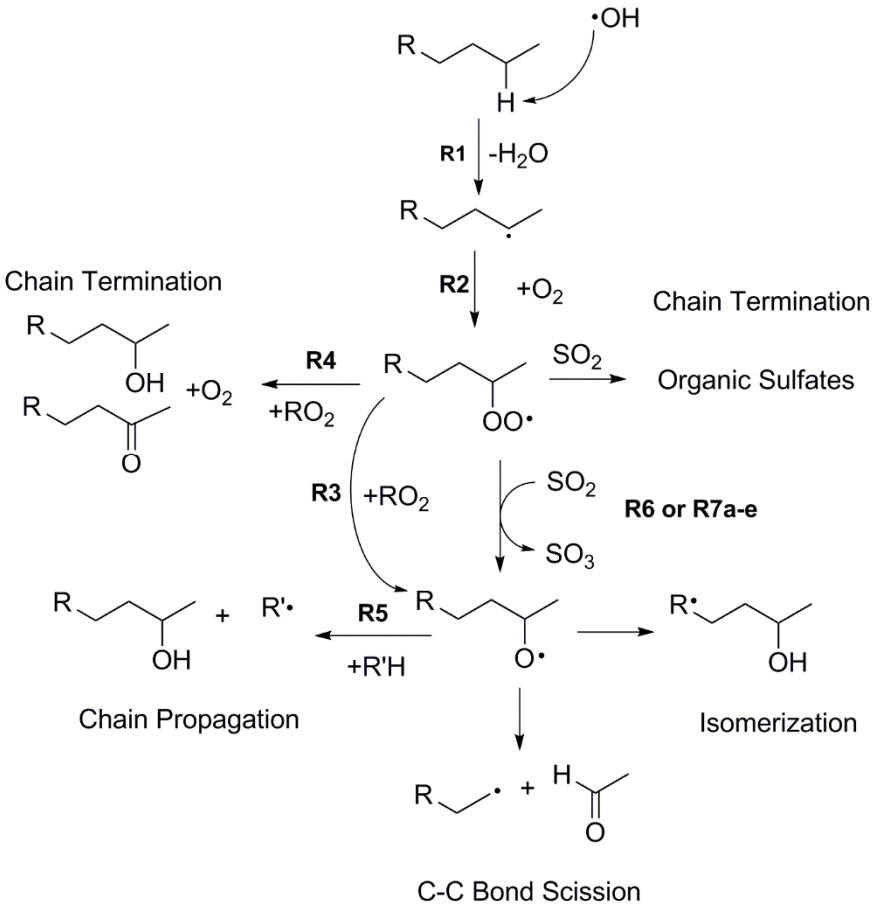
•OH
R
H
R1
-H2O
R
R2
+O2
Chain Termination
Chain Termination
R
OH
+O2
R
O
R4
+RO2
R
OO•
SO2
Organic Sulfates
R3
+RO2
SO2
SO3
R6 or R7a-e
R
OH
+
R'•
R5
+R'H
R
O•
R•
OH
Chain Propagation
Isomerization
R•
+
H
O
C-C Bond Scission

Fig. 1

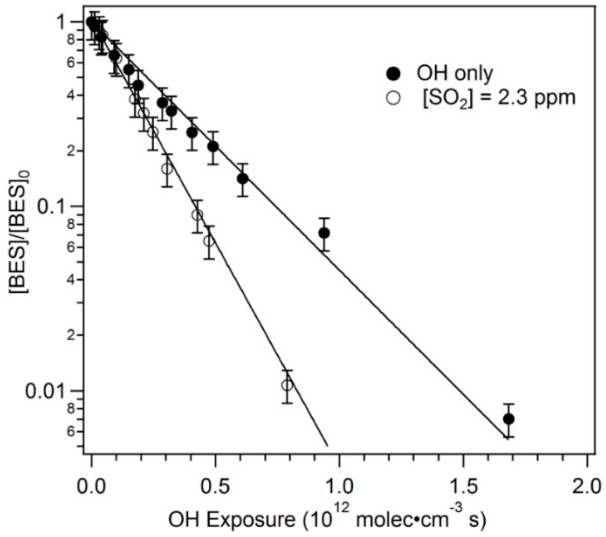
OH only
[SO2] = 2.3 ppm
[BES]/[BES]0
OH Exposure (10^12 molec•cm^-3 s)
1
0.1
0.01
0.0
0.5
1.0
1.5
2.0

Fig. 2

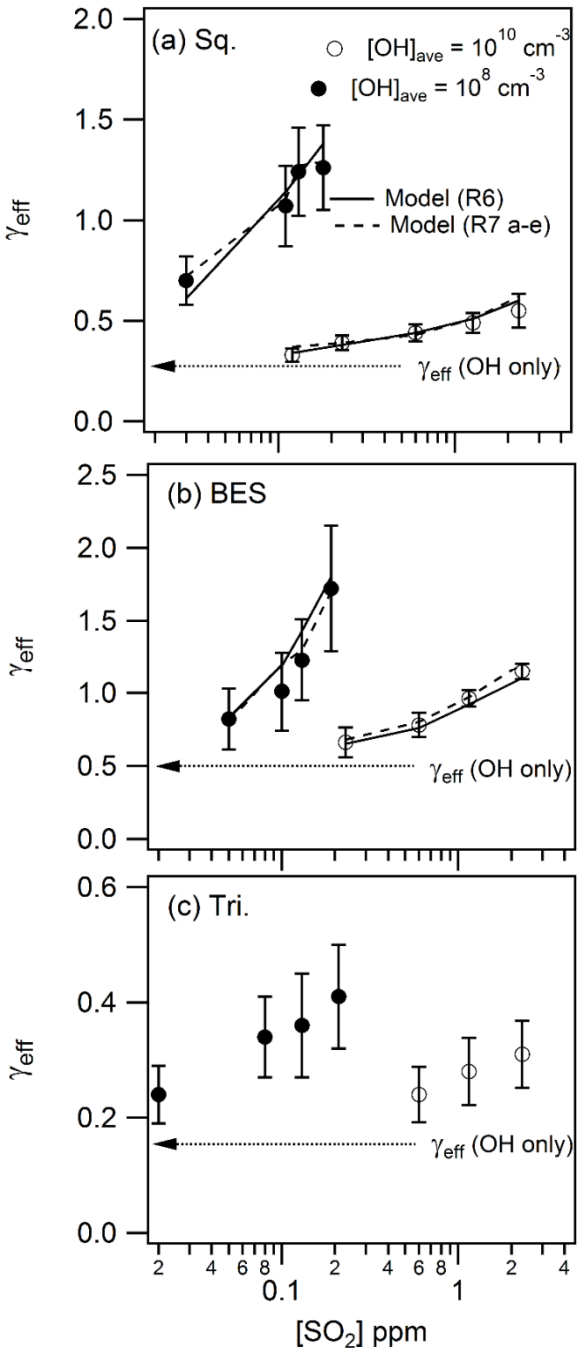
(a) Sq.
[OH]ave = 10^10 cm^-3
[OH]ave = 10^8 cm^-3
Model (R6)
Model (R7 a-e)
γeff (OH only)
(b) BES
γeff (OH only)
(c) Tri.
γeff (OH only)
γeff
[SO2] ppm

Fig. 3

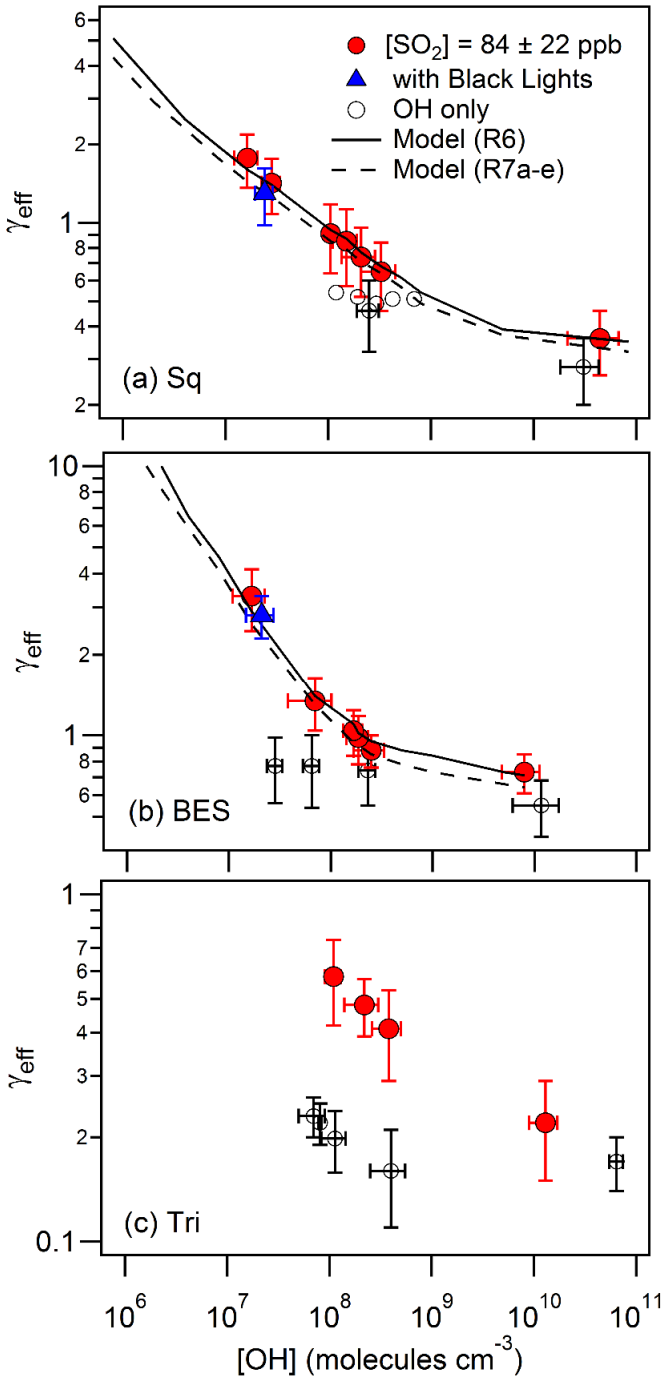
[SO2] = 84 ± 22 ppb
with Black Lights
OH only
Model (R6)
Model (R7a-e)
γeff
(a) Sq
(b) BES
(c) Tri
[OH] (molecules cm-3)

Fig. 4

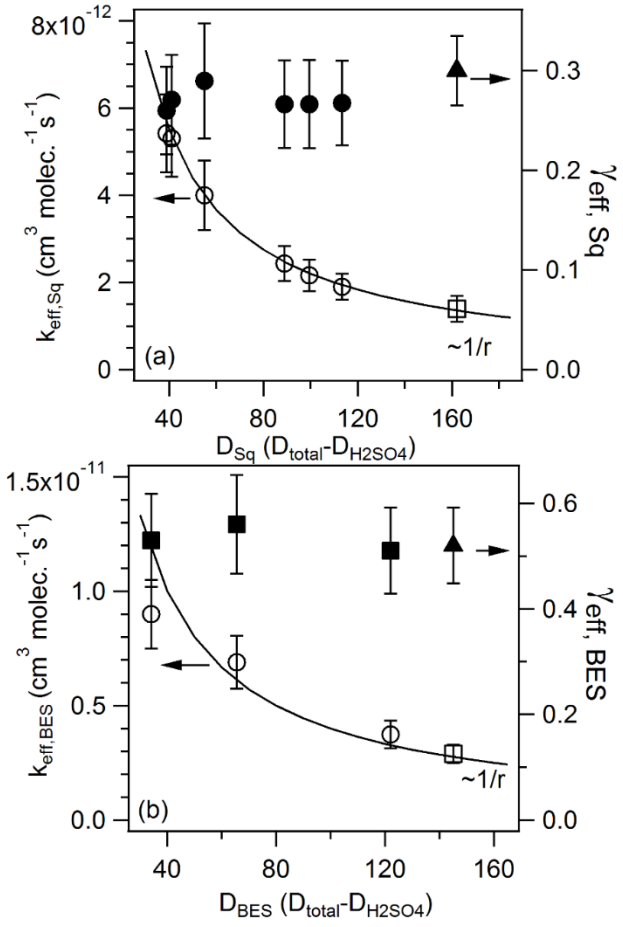
8x10^-12
6
4
2
0
k_eff,Sq (cm^3 molec.^-1 s^-1)
(a)
~1/r
0.3
0.2
0.1
0.0
γ_eff, Sq
40
80
120
160
D_Sq (D_total-D_H2SO4)
1.5x10^-11
1.0
0.5
0.0
k_eff,BES (cm^3 molec.^-1 s^-1)
(b)
~1/r
0.6
0.4
0.2
0.0
γ_eff, BES
40
80
120
160
D_BES (D_total-D_H2SO4)

Fig. 5

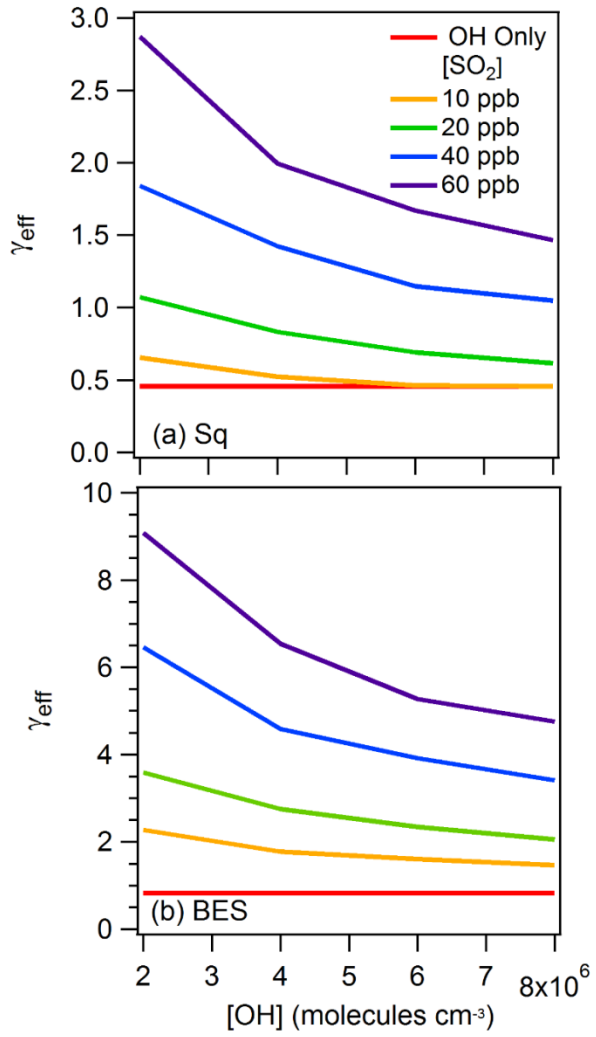
3.0
2.5
2.0
1.5
1.0
0.5
0.0
γeff
OH Only
[SO2]
10 ppb
20 ppb
40 ppb
60 ppb
(a) Sq
10
8
6
4
2
0
γeff
(b) BES
2
3
4
5
6
7
8x10^6
[OH] (molecules cm-3)

Fig. 6